Essentially Compact Schemes for Unsteady Viscous Incompressible Flows

Weinan E[*],[1] and Jian-Guo Liu[†],[2]

*School of Mathematics, Institute for Advanced Study, Princeton, New Jersey 08540 and †Department of Mathematics, Temple University, Philadelphia, Pennsylvania 19122

A new fourth-order accurate finite difference scheme for the computation of unsteady viscous incompressible flows is introduced. The scheme is based on the vorticity-stream function formulation. It is essentially compact and has the nice features of a compact scheme with regard to the treatment of boundary conditions. It is also very efficient, at every time step or Runge–Kutta stage, only two Poisson-like equations have to be solved. The Poisson-like equations are amenable to standard fast Poisson solvers usually designed for second order schemes. Detailed comparison with the second-order scheme shows the clear superiority of this new fourth-order scheme in resolving both the boundary layers and the gross features of the flow. This efficient fourth-order scheme also made it possible to compute the driven cavity flow at Reynolds number 10^6 on a 1024^2 grid at a reasonable cost. Fourth-order convergence is proved under mild regularity requirements. This is the first such result to our knowledge. © 1996 Academic Press, Inc.

1. INTRODUCTION

Compact schemes have attracted a considerable amount of attention recently in the area of viscous incompressible flow calculations. Ideally these schemes offer two attractive features: high order accuracy and small stencil. Consequently the number of numerical boundary conditions needed is considerably reduced, compared with standard high order schemes. This is of great importance for the computation of viscous incompressible flows for which numerical boundary conditions have always been an issue.

There has been numerous work on the construction of compact schemes for the incompressible Navier–Stokes equations (see, for example, [8, 3, 13]). The most noted ones include the work of Gupta [8] and Dennis *et al.* [3]. Almost all of these schemes are geared toward steady flow calculations even though the ideas may in principle be applied to unsteady flows as well. In the case of steady flows, these schemes have shown a great deal of potential [13].

As we emphasized repeatedly in [4], a basic design principle for finite difference schemes in vorticity-stream function formulation is to avoid coupling between the vorticity boundary condition and interior field equations. In this regard, the nonlinear convection terms present a problem for designing compact schemes. In [3, 8], this difficulty was overcome by using an appropriate change of variables. While accomplishing the task of obtaining compact differencing formulas for the convective terms, this trick also introduces a considerable amount of complexity into the scheme. This greatly limits the feasibility of these schemes.

The main purpose of this paper is to introduce a simple and efficient fourth-order scheme which overcomes all these difficulties. One main idea is the following. Since the simultaneous presence of the convection and viscous terms makes it difficult to construct simple and efficient compact schemes which fit nicely the structure of both the momentum equation and the kinematic constraint, it is natural to relax slightly the requirement of compactness (for the convection terms) so long as it does not complicate the treatment of the boundary conditions. The scheme we construct below is essentially compact and retains all the nice features of compact schemes. Specifically, this new scheme has the following features:

(1) It is almost explicit. For 2D problems, only two Poisson or Helmholtz equations are solved at each time step or each stage of the Runge–Kutta method. This changes to six Poisson solves for 3D problems. No iteration is required between the boundary values of vorticity and the interior field variables. Furthermore, the Poisson and Helmholtz equations can be solved using standard fast Poisson solvers designed for second-order schemes.

(2) The scheme is very simple and easy to implement. The complexity of the scheme is essentially the same as that of a standard second-order scheme. The simplicity of this scheme enables us to prove rigorously convergence with fourth-order accuracy. This is the first such result known to us.

The simplicity of this method also makes it very attrac-

[1] Current address: Courant Institute, New York University, New York, NY 10012. Email: weinan@cims.nyu.edu.
[2] Email: jliu@math.temple.edu.

tive for implementation on parallel machines. The compactness of the stencil means that very little information needs to be passed between different processors.

This new scheme also compares well with spectral methods. It has the advantage of being simple, robust, efficient, and much more stable. It is well known that if the viscous term is treated explicitly, the stability constraint for time steps associated with a Chebyshev method has the form: $\nu(\Delta t/\Delta x^4) \leq$ Const, whereas for our method the time step restriction coming from the diffusion term has the form $\nu(\Delta t/\Delta x^2) \leq$ Const. Consequently most calculations with Chebyshev methods use implicit treatment of the viscous term. To be fair we should also mention that Chebyshev methods also have the feature that they cluster much more points on the boundary. So they resolve boundary layers better than finite difference methods on uniform grids. On the other hand for high Reynolds number flows, it is not clear that boundary layer is the most difficult part to resolve. Aside from that, while fourth-order schemes are in theory less accurate than spectral methods, the difference can only be seen at a very high level of accuracy [12]. For most problems of practical interest, the fourth-order methods are comparable in accuracy with the spectral method [12].

Another important issue is whether the method has any cell Reynolds number constraint. As was discussed in [4], because of the fourth-order Runge–Kutta time-stepping procedure we use, coupled with a centered type of scheme in space, this new method does not have any cell Reynolds number constraint. In fact, for the calculations presented in Section 3, the cell Reynolds number will be as high as 10^3.

There are several competing ways of making fourth-order schemes in the literature [11, 9, 18, 19]. Among them, [9, 11] use the velocity-pressure formulation and the technique of applying the differentiated PDEs at the boundary. [18] uses the vorticity-streamfunction formulation with Hermite interpolation and second order formulas at the boundary. [19] also uses vorticity-streamfunction formulation and one-sided differences at the boundary. One can even extrapolate the results of a second-order scheme to get fourth-order accuracy [20]. A fair and detailed comparison of how well these different schemes actually perform is not an easy task and can only be left for future work.

The rest of this paper is organized as follows. In Section 2 we describe the scheme. In Section 3 we show our preliminary numerical results. We make a fairly detailed comparison of this new fourth-order scheme with the classical second-order scheme using the example of driven cavity flow. Our results show a clear superiority of this fourth-order scheme in resolving both the boundary layers and the gross features of the flow. We also show the numerical results computed on a 1024^2 grid at Reynolds number 10^6. The convergence results are proved in Section 4. Some remarks are made in Section 5.

2. DESCRIPTION OF THE SCHEME

We center our discussion on 2D problems. The scheme can be extended naturally to 3D, provided we use the vorticity-vector potential formulation. Since it requires much more notations we will postpone that to [5].

Our starting point is the incompressible Navier–Stokes equation in vorticity-stream function formulation

$$\frac{\partial \omega}{\partial t} + (\mathbf{u} \cdot \nabla)\omega = \nu \Delta \omega,$$
$$\Delta \psi = \omega, \tag{2.1}$$

with the boundary condition

$$\psi = 0, \quad \frac{\partial \psi}{\partial \mathbf{n}} = 0. \tag{2.2}$$

Here ψ is the stream function, $\mathbf{u} = (u, v) = (-\psi_y, \psi_x)$ is the velocity, and $\omega = -u_y + v_x$ is the vorticity. We can easily include forcing or inhomogeneous boundary conditions.

We first discuss the treatment of the Stokes part, treating the nonlinear convection terms as if they were some known forcing functions. We will use the notation: $f = \partial_x(u\omega) + \partial_y(v\omega)$ and write the first equation in (2.1) as

$$\frac{\partial \omega}{\partial t} = \nu \Delta \omega - f. \tag{2.3}$$

The most obvious and well-known compact discretization of (2.3) is

$$\left(1 + \frac{h^2}{12}\Delta_h\right)\frac{\partial \omega}{\partial t} = \nu\left(\Delta_h + \frac{h^2}{6}D_x^2 D_y^2\right)\omega$$
$$- \left(1 + \frac{h^2}{12}\Delta_h\right)f. \tag{2.4}$$

Here Δ_h is the standard 5-point formula for Δ, and the operators D_x^2, D_y^2 are defined by

$$(D_x^2 g)(x, y) = \frac{g(x + h, y) - 2g(x, y) + g(x - h, y)}{h^2}$$

$$(D_y^2 g)(x, y) = \frac{g(x, y + h) - 2g(x, y) + g(x, y - h)}{h^2}.$$

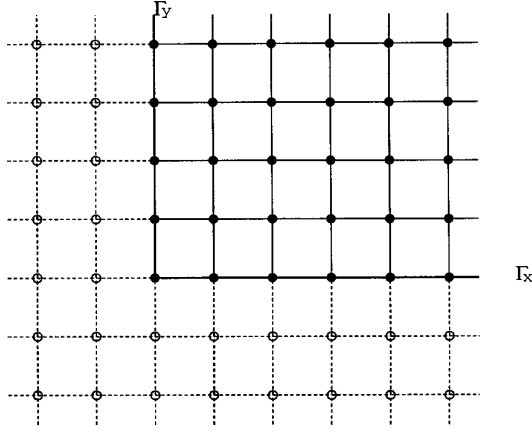In the following, we will also use the notation

E AND LIU

FIG. 1 The numerical grid: "ghost points" are shown in "Circ."

$$(\tilde{D}_x g)(x, y) = \frac{g(x + h, y) - g(x - h, y)}{2h}$$

$$(\tilde{D}_y g)(x, y) = \frac{g(x, y + h) - g(x, y - h)}{2h}.$$

We have assumed, without loss of generality, that $\Delta x = \Delta y = h$.

Equation (2.4) is a $O(h^4)$ approximation to (2.3). Similarly, we discretize the second equation in (2.1) using

$$\left(\Delta_h + \frac{h^2}{6} D_x^2 D_y^2\right)\psi = \left(1 + \frac{h^2}{12}\Delta_h\right)\omega. \qquad (2.5)$$

So far it has been completely standard. We now come to the boundary conditions. Assume that the mesh is as depicted in Fig. 1. It is natural to supplement (2.5) with the condition of no normal flow:

$$\psi|_\Gamma = 0.$$

In order to obtain the numerical values at the "ghost points" outside the physical domain Ω, we use the no-slip condition $\partial\psi/\partial\mathbf{n}|_\Gamma = 0$ twice at the physical boundary $\Gamma = \Gamma_x \cup \Gamma_y$: once using a fourth-order one-sided approximation; once using a fourth-order centered approximation. For example, at the boundary Γ_y we have

$$\left(\frac{\partial\psi}{\partial x}\right)_{0,j} \approx \frac{-3\psi_{-1,j} - 10\psi_{0,j} + 18\psi_{1,j} - 6\psi_{2,j} + \psi_{3,j}}{12h} \qquad (2.6)$$

$$\left(\frac{\partial\psi}{\partial x}\right)_{0,j} \approx \frac{\psi_{-2,j} - 8\psi_{-1,j} + 8\psi_{1,j} - \psi_{2,j}}{12h}. \qquad (2.7)$$

Consequently, we have

$$\psi_{-1,j} = 6\psi_{1,j} - 2\psi_{2,j} + \frac{1}{3}\psi_{3,j} - 4h\left(\frac{\partial\psi}{\partial x}\right)_{0,j} \qquad (2.8)$$

$$\psi_{-2,j} = 40\psi_{1,j} - 15\psi_{2,j} + \frac{8}{3}\psi_{3,j} - 20h\left(\frac{\partial\psi}{\partial x}\right)_{0,j}. \qquad (2.9)$$

To evaluate the vorticity at the boundary, we use a fourth-order approximation of $\omega = \Delta\psi = \psi_{xx}$:

$$\omega_{0,j} = \frac{1}{12h^2}\left(16(\psi_{-1,j} + \psi_{1,j}) - (\psi_{-2,j} + \psi_{2,j})\right). \qquad (2.10)$$

Using (2.8)–(2.9), we obtain

$$\omega_{0,j} = \frac{108\psi_{1,j} - 27\psi_{2,j} + 4\psi_{3,j}}{18h^2} - \frac{11}{3h}\left(\frac{\partial\psi}{\partial x}\right)_{0,j}. \qquad (2.11)$$

This is known as Briley's formula [1].

Now the velocity $\mathbf{u} = (u, v)$ can be evaluated readily at all interior grid points by using the standard fourth-order accurate formulas,

$$u = -\tilde{D}_y\left(1 - \frac{h^2}{6} D_y^2\right)\psi, \quad v = \tilde{D}_x\left(1 - \frac{h^2}{6} D_x^2\right)\psi, \qquad (2.12)$$

or some standard compact difference operators. On the boundary Γ, we use naturally

$$u = 0, \quad v = 0. \qquad (2.13)$$

To treat the convection terms, we note that

$$\left(1 + \frac{h^2}{12}\Delta_h\right)\tilde{D}_x\left(1 - \frac{h^2}{6} D_x^2\right) = \tilde{D}_x\left(1 + \frac{h^2}{6} D_y^2\right)$$
$$- \frac{h^2}{12}\Delta_h\tilde{D}_x + O(h^4). \qquad (2.14)$$

Hence we can approximate $(1 + (h^2/12)\Delta_h) f$ to fourth-order using

$$\left(1 + \frac{h^2}{12}\Delta_h\right)f$$

$$= \left(1 + \frac{h^2}{12}\Delta_h\right)\left\{\tilde{D}_x\left(1 - \frac{h^2}{6} D_x^2\right)(u\omega)\right.$$

$$\left. + \tilde{D}_y\left(1 - \frac{h^2}{6} D_y^2\right)(v\omega)\right\} + O(h^4)$$

$$= \tilde{D}_x\left(1 + \frac{h^2}{6} D_y^2\right)(u\omega) + \tilde{D}_y\left(1 + \frac{h^2}{6} D_x^2\right)(v\omega) \qquad (2.15)$$

$$-\frac{h^2}{12}\Delta_h(\tilde{D}_x(u\omega) + \tilde{D}_y(v\omega)) + O(h^4)$$

$$= \tilde{D}_x\left(1 + \frac{h^2}{6}D_y^2\right)(u\omega) + \tilde{D}_y\left(1 + \frac{h^2}{6}D_x^2\right)(v\omega)$$

$$-\frac{h^2}{12}\Delta_h(u\tilde{D}_x\omega + v\tilde{D}_y\omega) + O(h^4).$$

The operator appearing in the first term of the right-hand side of (2.15) has a 9-point compact stencil and so does the operator in the second term. The third term, however, is not compact. Nevertheless this does not present any problem computationally for two reasons: In the interior of the domain (for $i, j \geq 2$), this term can be evaluated very efficiently since the convection terms will be treated explicitly in the fully discrete scheme. Near the boundary (i, or $j = 1$), we need the boundary value of $u\tilde{D}_x\omega + v\tilde{D}_y\omega$ on Γ. In the present case, we can set

$$u\tilde{D}_x\omega + v\tilde{D}_y\omega|_\Gamma = 0 \qquad (2.16)$$

and still preserve fourth-order accuracy. More generally, given u, v, and ω, it is easy to evaluate $u\tilde{D}_x\omega + v\tilde{D}_y\omega$ at the boundary with second-order accuracy. For example, if Γ is a wall we must have $v = 0$. Hence $u\tilde{D}_x\omega + v\tilde{D}_y\omega = u\tilde{D}_x\omega$ which can be readily computed. If Γ is an in- or outflow boundary, we can often specify the values of vorticity near Γ. Therefore, $u\tilde{D}_x\omega + v\tilde{D}_y\omega$ can again be easily computed. These will be discussed in more detail later.

Finally, we discuss the temporal discretization procedure. For simplicity we will present the forward Euler time-discretization. The extension to multistep or Runge–Kutta methods is straightforward. In the computations presented below we use the classical fourth-order Runge–Kutta method.

Initialization: Given $\{\omega_{ij}^0\}$, compute

$$\left(1 + \frac{h^2}{12}\Delta_h\right)\omega^0 = \overline{\omega}^0 \qquad (2.17)$$

Time-stepping. Given $\{\omega_{ij}^n\}$, we compute $\{\omega_{ij}^{n+1}\}$ via the following steps.

Step 1. Update $\{\overline{\omega}_{i,j}^{n+1}\}_{i\geq 1, j\geq 1}$ using

$$\frac{\overline{\omega}^{n+1} - \overline{\omega}^n}{\Delta t} + \tilde{D}_x\left(1 + \frac{h^2}{6}D_y^2\right)(u^n\omega^n)$$

$$+ \tilde{D}_y\left(1 + \frac{h^2}{6}D_x^2\right)(v^n\omega^n) \qquad (2.18)$$

$$-\frac{h^2}{12}\Delta_h(u^n\tilde{D}_x\omega^n + v^n\tilde{D}_y\omega^n)$$

$$= \nu\left(\Delta_h + \frac{h^2}{6}D_x^2D_y^2\right)\omega^n$$

Step 2. Solve for $\{\psi_{i,j}^{n+1}\}_{i\geq 1, j\geq 1}$ using

$$\left(\Delta_h + \frac{h^2}{6}D_x^2D_y^2\right)\psi^{n+1} = \overline{\omega}^{n+1} \qquad (2.19)$$

with the boundary condition

$$\psi^{n+1}|_\Gamma = 0.$$

Compute ψ^{n+1} at the "ghost points" using (2.8).

Step 3. Solve for $\{\omega_{i,j}^{n+1}\}_{i\geq 1, j\geq 1}$ using

$$\left(1 + \frac{h^2}{12}\Delta_h\right)\omega^{n+1} = \overline{\omega}^{n+1} \qquad (2.20)$$

with the boundary condition (2.11).

Step 4. Update the velocity using

$$u^{n+1} = -\tilde{D}_y\left(1 - \frac{h^2}{6}D_y^2\right)\psi^{n+1},$$

$$\qquad (2.21)$$

$$v^{n+1} = \tilde{D}_x\left(1 - \frac{h^2}{6}D_x^2\right)\psi^{n+1},$$

or some compact fourth-order differencing [2] for $i, j \geq 1$, and $u^{n+1}|_\Gamma = 0$, $v^{n+1}|_\Gamma = 0$.

The efficiency of this method is obvious. Unlike most other schemes based on vorticity-stream function formulation, here there is no need to iterate between the boundary values of vorticity and the interior field variables. Only two Poisson-like equations, namely (2.19) and (2.20), are solved at each step or each stage of the Runge–Kutta method. Both can be solved using standard fast Poisson solvers.

The changes needed for the case $\Delta x \neq \Delta y$ are essentially obvious:

$$\Delta_h + \frac{h^2}{6}D_x^2D_y^2 \quad \text{changes to } \Delta_h + \frac{1}{12}(\Delta x^2 + \Delta y^2)D_x^2D_y^2,$$

$$1 + \frac{h^2}{12}\Delta_h \quad \text{changes to } 1 + \frac{1}{12}(\Delta x^2 D_x^2 + \Delta y^2 D_y^2),$$

$$1 + \frac{h^2}{6}D_x^2 \quad \text{changes to } 1 + \frac{\Delta x^2}{6}D_x^2,$$

$$1 + \frac{h^2}{6} D_y^2 \quad \text{changes to } 1 + \frac{\Delta y^2}{6} D_y^2.$$

Likewise, external forcing can be incorporated in a trivial way. Another extension which we need below for the driven cavity flow is the case when the physical boundary slips. In this case (2.16) is no longer consistent. However, an easy modification of (2.16) is sufficient. Take the case when Γ_x slips with velocity $u_b(x)$:

$$u = u_b(x), \quad v = 0$$

on Γ_x. In this case

$$u\tilde{D}_x\omega + v\tilde{D}_y\omega|_\Gamma = u_b(x)\tilde{D}_x\omega$$

which can be readily computed since $\omega|_{\Gamma_x}$ is known.

At boundaries where there is an in- or out-flow, the formulas should be modified. For clarity, we first present the modification for Thom's formula coupled with the standard second-order scheme [4]. The homogeneous Dirichlet boundary condition (2.2) changes into

$$\psi^{n+1}|_\Gamma = \psi_{bc}, \quad \psi_{bc}(s) = \int_0^s u_\mathbf{n}\, ds, \qquad (2.22)$$

where s parametrizes the boundary, $u_\mathbf{n}$ is the normal component of $\mathbf{u}$. Using the above relation, we get

$$\omega_{i,0} = \Delta_h \psi_{i,0} = \frac{\psi_{i,1} - 2\psi_{i,0} + \psi_{i,-1}}{h^2} + \partial_x v(x_i) + O(h^2).$$

Thom's formula becomes

$$\omega_{i,0} = 2\frac{\psi_{i,1} - \psi_{bc}(x_i)}{h^2} + \frac{2}{h} u_{bc}(x_i) + \partial_x v_{bc}(x_i). \quad (2.23)$$

Similarly for the fourth-order scheme, the vorticity boundary condition (2.11) changes to

$$\omega_{i,0} = \frac{108\psi_{i,1} - 27\psi_{i,2} + 4\psi_{i,3} - 125\psi_{bc}(x_i)}{18h^2}$$
$$- \frac{11}{3h} u_{bc}(x_i) + \partial_x v(x_i)$$

and (2.16) becomes

$$u\tilde{D}_x\omega + v\tilde{D}_y\omega|_\Gamma = u_b(x)\tilde{D}_x\omega + v_b(x)\overline{D}_y\omega,$$

where $\overline{D}_y$ is a second-order accurate one-sided approximation to ∂_y.

This scheme is named essentially compact (EC4 for short) since the only noncompact part occurs in the treatment of the convection terms, and the noncompact differencing does not increase the need for numerically supplemented boundary conditions. So the most attractive features of the compact schemes are retained. Only one one-sided formula (2.6) is used. The rest are centered differences. This is the minimum number of one-sided formulas one can get away with for a fourth-order scheme [22]. This feature of our scheme greatly simplifies the analysis presented below. We should remark that clever use of one-sided differences in the convection terms might lead to a better method for high Reynolds number flows. But this is a different level of issue and will not be addressed here.
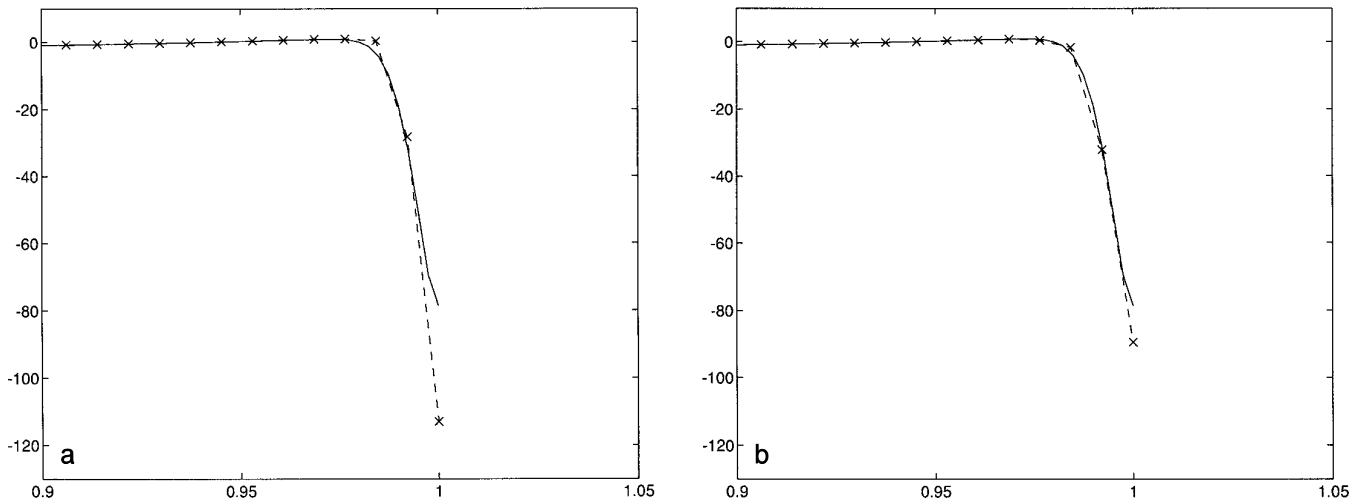
3. NUMERICAL RESULTS

We implemented EC4 on the SPARC station and the C-90 at Pittsburgh Supercomputing Center, for both 2D and 3D problems. Here we report an example of our 2D computation—the driven cavity flow. Numerical results for 3D will be presented in [5].

We used the classical fourth-order Runge–Kutta method to discretize time. We tested numerically that the CFL number ($=\max\{\nu(\Delta t/\Delta x^2), |u|_\infty(\Delta t/\Delta x)\}$) for the fully nonlinear code is about 1.8125. The Poisson and Helmholtz equations are solved using FFT. The fourth-order accuracy of the code is checked by putting in different kinds of functions satisfying the Navier–Stokes equation with appropriate forcing.

We will center our discussion on the comparison between EC4 and the standard second-order scheme (with Thom's formula as the vorticity boundary condition). The details of this second-order method and its efficient implementation was discussed in [4]. For the present discussion it is only necessary to know that the implementation of these two methods are very similar: both use fourth-order Runge–Kutta in time and FFT to solve the Poisson-like equations. In fact the EC4 code was a small modification of the second-order code. The flow domain is $[0, 1] \times [0, 1]$, with the no-slip condition imposed. The upper boundary moves with velocity $u_b(x)$. Most of our results are computed with $u_b(x) = 16x^2(1 - x)^2$ and initial data: $\psi_0(x, y) = (y^2 - y^3)u_b(x)$. These results will be presented in Sections 3.1–3.3. We have also tried the more conventional boundary condition $u_b(x) = 1$ with impulsive start. These results will be presented in Section 3.4.

3.1. *Ability to Resolve the Boundary Layers*

One major difficulty in the computation of high Reynolds number incompressible flows is the resolution of the viscous boundary layer. The thickness of the boundary layer is on the order of $\sqrt{\nu}$ (in dimensionless units) which is comparable to the smallest active scale in a 2D incompressible flow [9]. This viscous boundary layer has to be

FIG. 2. (a) Resolution of the boundary layer for the second order scheme. Shown in the figure are the horizontal cuts of vorticity at $y = 0.5$. The solid line is the numerically converged solution computed on a 400^2 grid. The dashed line is computed on a 128^2 grid using the second-order scheme. Other parameters: $\nu = 10^{-4}$, $t = 2$. (b) Resolution of the boundary layer for EC4. Shown in the figure are the horizontal cuts of vorticity at $y = 0.5$. The solid line is the numerically converged solution computed on a 400^2 grid. The dashed line is computed on a 128^2 grid using EC4. Other parameters: $\nu = 10^{-4}$, $t = 2$.

resolved to some extent since it separates eventually and the vortical structures generated from the separation drastically influence the overall flow.

In Figs. 2a and 2b we plot the numerically computed vorticity field using respectively the second-order scheme and EC4 at a horizontal cut $\{y = 0.5\}$ at $t = 2$. Both computations are done on a 128^2 grid with $\nu = 10^{-4}$. The solid line is the numerically converged solution computed using the second-order method on a 400^2 grid. The superiority of EC4 in resolving the boundary layer is rather clear. While both solutions on the coarse grid undershoot in the boundary layer, the solution given by EC4 undershoots much less than the one given by the second-order scheme. Moreover, there is also an appreciable amount of overshoot in the solution of the second-order scheme.

Another sign for EC4's ability to better resolve the boundary layer is displayed in Fig. 3a and 3b, where we compare the contour plots of the numerically computed vorticity field using, respectively, the second-order scheme and EC4 on a 100^2 grid. Mesh-scale oscillations can be seen quite clearly in Fig. 3a for the second-order scheme, but not in Fig. 3b for EC4. We should remark that in this case the flow is only marginally resolved for EC4, but it is not resolved by any reasonable standards for the second-order scheme.

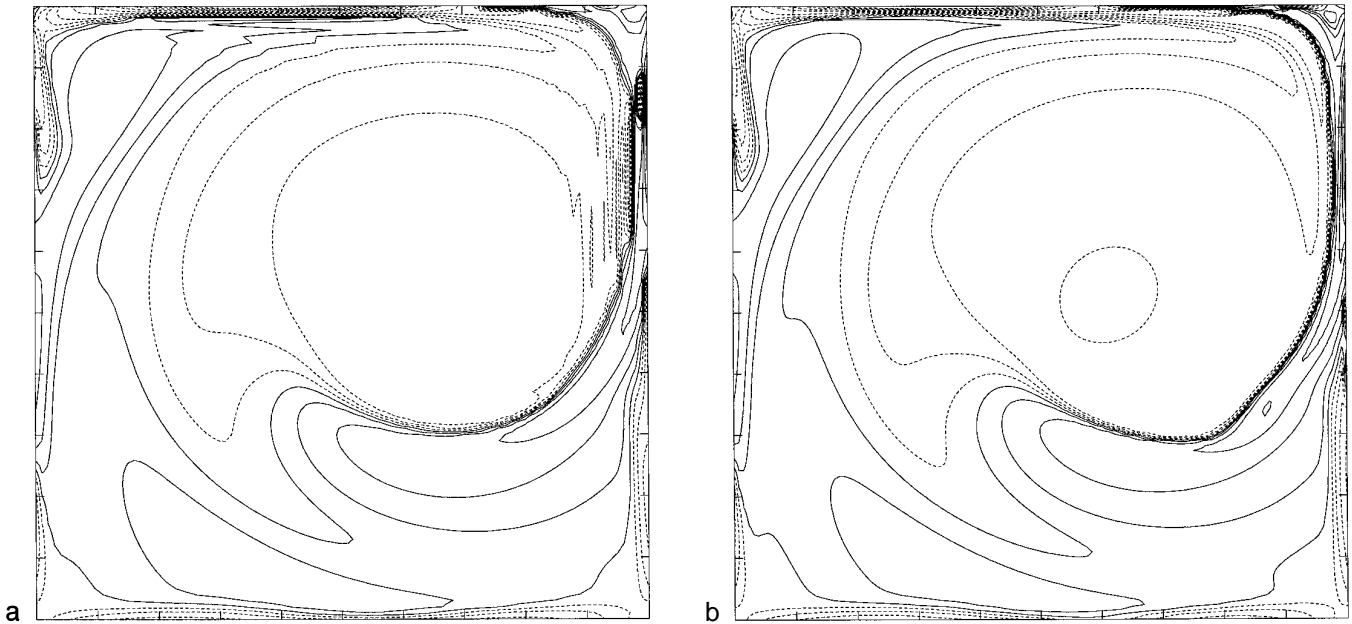### 3.2. Ability to Resolve Gross Features of the Flow

In this category we will only present one piece of evidence displayed in Figs. 4a–c. These three figures look very similar, except for one important difference. In the numerically converged solution plotted in Fig. 4a, the vor-

tex at the lower right corner has a bump on one side. This bump is clearly reproduced in Fig. 4b which is the result of a calculation using EC4 on a 96^2 grid. However, this feature is missed entirely in Fig. 4c, which shows the result of the second-order scheme on a 128^2 grid.

3.3. Numerical Result of the Driven Cavity Flow at Reynolds Number 10^6 Computed on a 1024^2 Grid

Most important among all of these features is the exciting possibility brought by this new efficient fourth-order scheme to resolve flows at higher Reynolds number. In [4] we computed the driven cavity flow at Reynolds number 10^5 using the second-order scheme on a 1024^2 grid (which is typically what we can do with our modest computing budget). Attempts to compute the flow at Reynolds number 10^6 failed since numerical solution quickly turns into noise. With EC4, we have been able not only to confirm these earlier results, but also to compute the driven cavity flow at Reynolds number 10^6. Below we report some of our results.

Figure 5 shows the vorticity contour at $t = 2$. This should be compared with Fig. 6 which shows the same information at Reynolds number 10^5. The initial and boundary conditions are the same. The overall structure appeared in both figures are very similar, but the vortices shed from the separated boundary layer at Reynolds number 10^6 are smaller. To examine the resolution of the boundary layers, we display in Fig. 7 the horizontal cut of vorticity at $y = 0.5$ near the right boundary $x = 1$, with "x" representing the values on the grid. The numerical solution displays a sharp transition at the boundary layer. Even though there

FIG. 3. (a) Vorticity contour of the numerical solution computed on a 100^2 grid using the second order scheme. Numerical oscillations can be clearly seen. Other parameters: $\nu = 10^{-4}$, $t = 2$. (b) Vorticity contour of the numerical solution computed on a 100^2 grid using EC4. There are no appreciable amount of numerical oscillations. Other parameters: $\nu = 10^{-4}$, $t = 2$.

are only three points across the boundary layer, the numerical solution does not contain any appreciable amount of oscillations away from the boundary. Near the boundary, there is an undershoot at the fourth grid point. Still the undershoot is remarkably small considering how sharp the transition is across the boundary. Clearly in the present case the flow is only marginally resolved. We carried out this computation up to $t = 10$ but so far we are only able to verify the results up to $t = 2$ on a 1600^2 grid.

We add a remark here about the cost of EC4. Our experience has shown consistently that EC4 costs less than three times the cost of the second-order scheme. For example, to compute the driven cavity flow at Re $= 10^5$ on a 1024^2 grid on C-90 at the Pittsburgh Supercomputing Center, with the same time steps, the second-order scheme takes 2067 s to advance from $t = 0$ to $t = 2$, EC4 takes 5628 s (both on a single processor).

3.4. Results for the case of $u_b(x) = 1$ with impulsive start

In Figs. 8a–b we compare the results computed using EC4 and the second-order method with $u_b(x) = 1$ and impulsive start at Reynolds number Re $= 10^4$. This is a standard test problem, particularly for the steady Navier–Stokes equations [7, 20]. The numerical parameters are set at: $t = 400$, CFL $= 1.5$, $h = \frac{1}{128}$. The two figures are very different, even in gross features. To find out which one is closer to the truth, we plot in Fig. 8c the results of the second-order code on a 256×256 grid. Clearly it is much
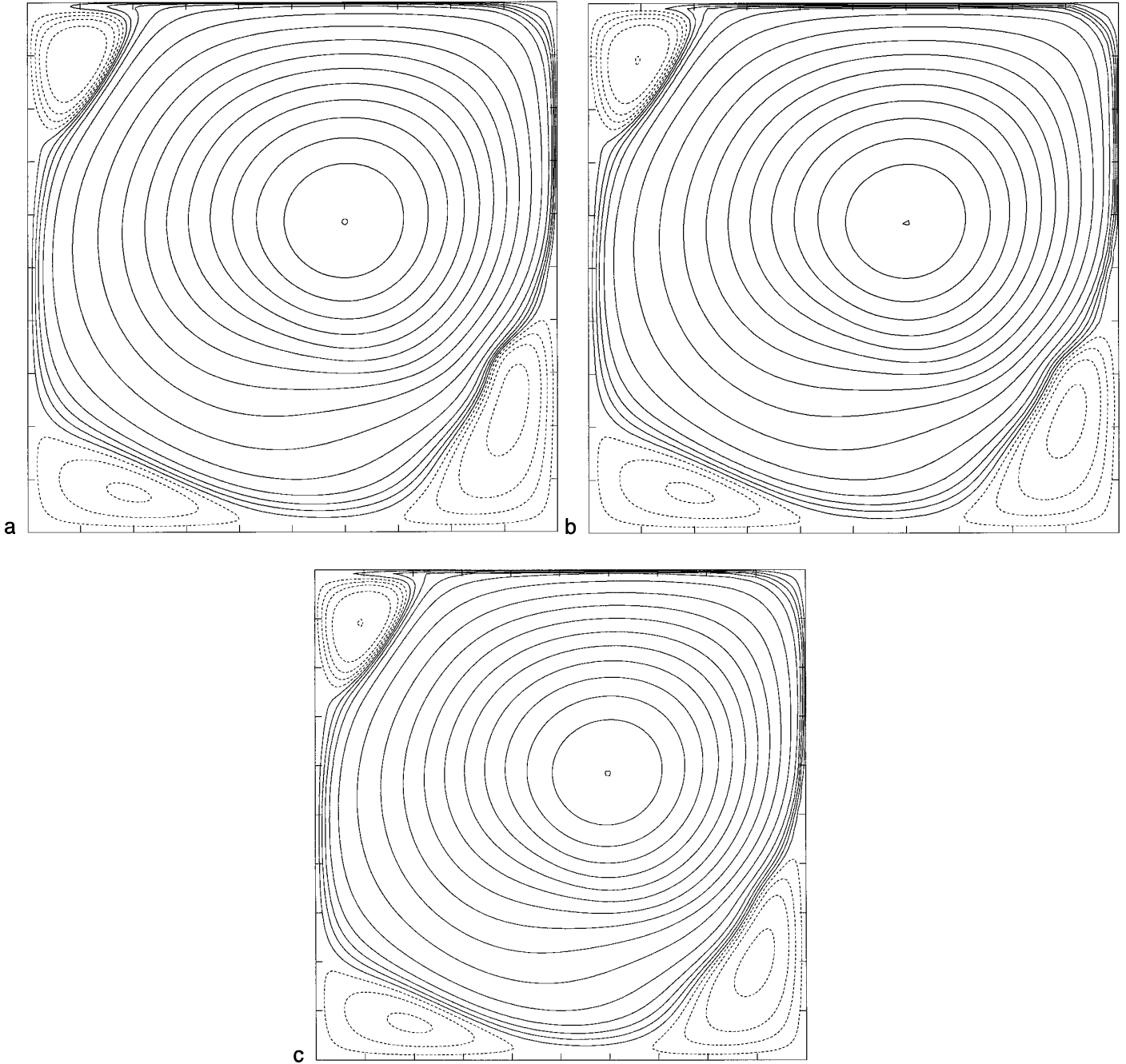
closer to Fig. 8b. These results also resemble closely the ones reported in [7, 20]. For the second-order scheme on a 128×128 grid, the numerical oscillations generated at the lid are so big that they lock the flow at an entirely wrong state.

4. PROOF OF FOURTH-ORDER CONVERGENCE FOR SMOOTH SOLUTIONS

Because of their complexity, it is usually very difficult to prove uniform convergence of high-order schemes when boundaries are involved. The compactness of our scheme presents considerable amount of simplification that enables us to give a fairly elegant proof of fourth-order convergence under mild regularity assumptions.

For simplicity of presentation we will work with the special case when $\Omega = [0, 1] \times [0, 1]$ with no-slip boundary condition at $\{y = 0, 1\}$ and periodic boundary condition at $\{x = 0, 1\}$. The associated numerical grid will be denoted by $\{x_i = i/N, y_j = j/N\}$ with $i = 0, 1, ..., N$ and $j = 0, 1, ..., N$. The periodicity condition in the x-direction means that there is no boundary term when we sum by parts over the i index. We will concentrate on the semi-discrete case. Extension to the fully discrete scheme is more or less straightforward. Extension to the case when we have different number of grid points in the x and y directions is trivial.

THEOREM. *For any* $\alpha > 0$, *let* $\psi_e \in L^\infty([0, T]; C^{6,\alpha}(\overline{\Omega}))$ *be the solution of the Navier–Stokes equation* (2.1)–

FIG. 4. Gross features of the flow. (a) Shown in the figure is the contour plot of stream function for the numerically converged solution computed on a 400^2 grid. Other parameters: $\nu = 10^{-4}$, $t = 2$. (b) Shown in the figure is the contour plot of stream function computed on a 96^2 grid using EC4. The bump on the lower right corner vortex is clearly reproduced. Other parameters: $\nu = 10^{-4}$, $t = 2$. (c) Shown in the figure is the contour plot of stream function computed on a 128^2 grid using the second order scheme. The bump on the lower right corner vortex is missing. Other parameters: $\nu = 10^{-4}$, $t = 2$.

(2.2) *and* $\mathbf{u}_h$ *be the approximate solution of* EC4; *then we have*

$$\sup_{0 \le t \le T} \|\mathbf{u}(\cdot, t) - \mathbf{u}_h(\cdot, t)\|_{L^2} \le Ch^4 \sup_{0 \le t \le T} \|\psi_e(\cdot, t)\|^2_{C^{6,\alpha}(\overline{\Omega})}.$$

Here we will prove fourth-order convergence under the assumption that the solution is as smooth as we want. The proof of the theorem as stated above goes along the same lines but is a bit more complicated. The details of that can be obtained directly from the authors.

The convergence proof follows the standard strategy of consistency and stability estimates. In the consistency part, we use the exact stream function as the starting point. Instead of directly comparing the numerical solutions with the exact velocity and vorticity, we compare them with the ones constructed from the exact stream function. The constructed discrete fields satisfy exactly the boundary conditions in the numerical scheme. The difference between these constructed fields and the exact ones are estimated in Lemma 4.1. The advantage of this approach is that all truncation errors are lumped into the momentum equation, no error terms appear in the boundary conditions. This simplifies the summation by parts used repeatedly in the stability part of the proof.

Analogous results for the second-order schemes were proved in a series of papers [16, 14, 10, 15]. The basic idea used in these papers is that once stability in L^2 is established for the linearized equations, convergence (together with convergence of derivatives) follows from the general result of Strang [21]. Our interest here is mainly to prove fourth-order convergence for the compact scheme. We are not aware of such result even for the heat equation when boundaries are present.

4.1. Consistency Analysis

Let $(\psi_e, u_e, v_e, \omega_e)(x, y, t)$ be the exact solution of the Navier–Stokes equation (2.1)–(2.2) and let $\hat{\psi}$ be a solution of

$$\Delta(\partial_t - \nu\Delta)\hat{\psi} = 0,$$

$$\hat{\psi} = 0, \quad \frac{\partial\hat{\psi}}{\partial y} = \frac{1}{20}\frac{\partial^5\psi_e}{\partial y^5}, \quad \text{on } \Gamma_x, \qquad (4.1)$$

$$\hat{\psi}(x, y, 0) = 0,$$

and $\hat{\omega} = \Delta\hat{\psi}$. Denote

$$\overline{\psi} = \psi_e + h^4\hat{\psi}, \quad \overline{\omega} = \omega_e + h^4\hat{\omega}. \qquad (4.2)$$

The correction terms associated with $\hat{\psi}$ and $\hat{\omega}$ are needed to get consistency at the boundary. This is a classical technique [6] necessary even for analyzing finite difference approximations for the Laplace equation with Dirichlet boundary condition when the physical boundary is not a grid line (see Appendix 2 of [4]).
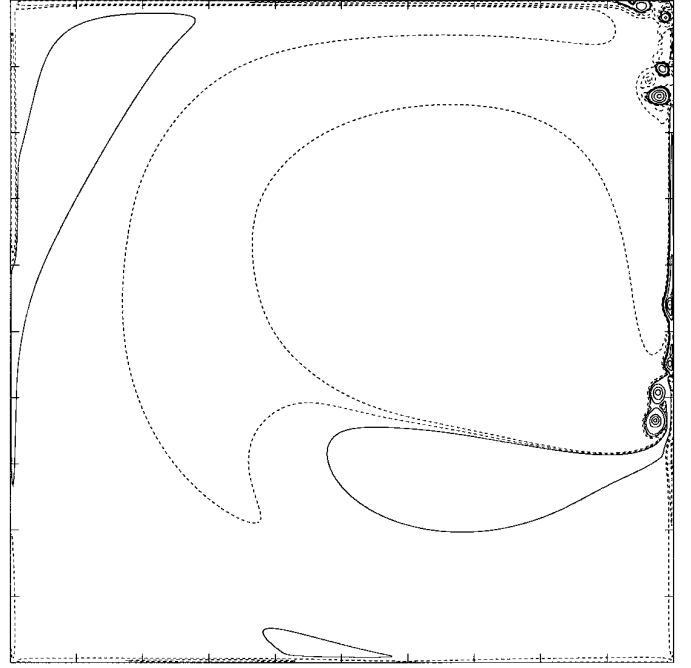
Let

$$\Psi_{i,j}(t) = \overline{\psi}(x_i, y_j, t), \qquad (4.4)$$

for $0 \leq i \leq N$, $0 \leq j \leq N$, and

$$\Psi_{i,-1} = 6\Psi_{i,1} - 2\Psi_{i,2} + \tfrac{1}{3}\Psi_{i,3}. \qquad (4.5)$$

Let

FIG. 5. Contour plot of vorticity at Reynolds number 10^6 computed using EC4. Other parameters: $n = 1024$, $t = 2$.

$$U_{i,j} = -\tilde{D}_y\left(1 - \frac{h^2}{6}D_y^2\right)\Psi_{i,j}, \quad V_{i,j} = \tilde{D}_x\left(1 - \frac{h^2}{6}D_x^2\right)\Psi_{i,j},$$

$$(4.6)$$

$$\overline{\Omega}_{i,j} = \left(\Delta_h + \frac{h^2}{6}D_x^2D_y^2\right)\Psi_{i,j} \qquad (4.7)$$

for $0 \leq i \leq N$, $1 \leq j \leq N - 1$, and let $\Omega_{i,j}$ be the solution of

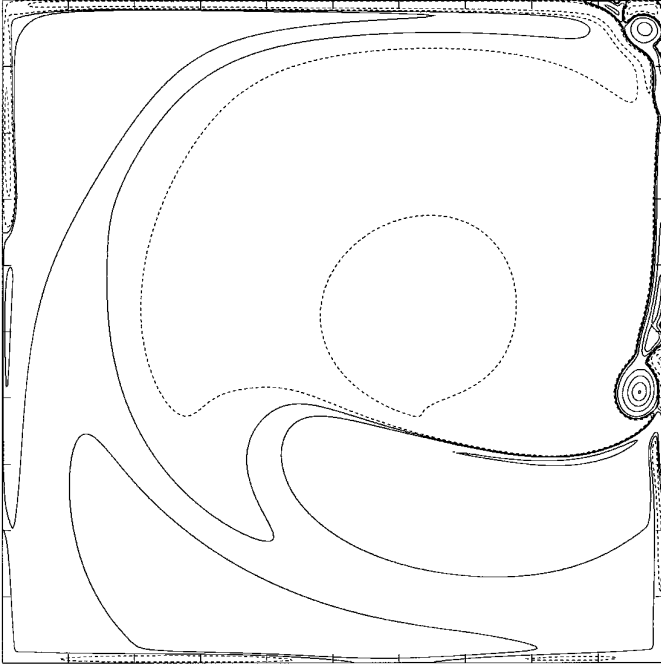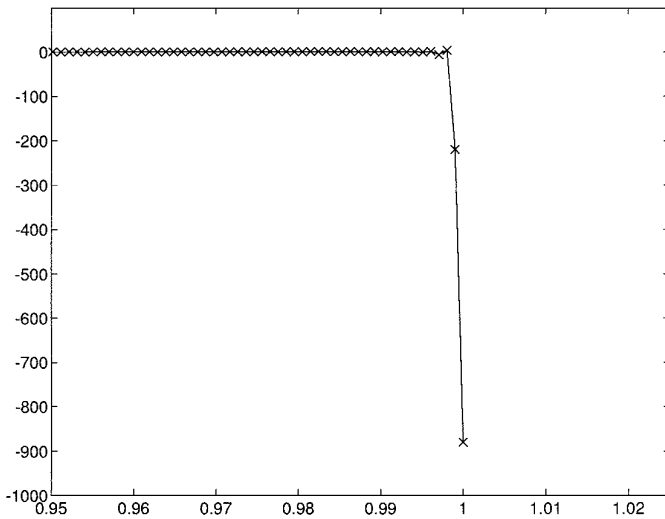$$\left(1 + \frac{h^2}{12}\Delta_h\right)\Omega_{i,j} = \overline{\Omega}_{i,j}, \qquad (4.8)$$

with the boundary condition:

$$\Omega_{i,0} = \frac{1}{18h^2}(108\Psi_{i,1} - 27\Psi_{i,2} + 4\Psi_{i,3}), \quad 0 \leq i \leq N, \quad (4.9)$$

and similarly for $\{\Omega_{i,N}\}$. It is helpful here to think of $\overline{\psi}$ as having been extended smoothly to a neighborhood of Ω: $\Omega_\delta = [0, 1] \times [-\delta, 1 + \delta]$, and still retaining periodicity in the x-variable. Such an extension is always possible.

LEMMA 4.1. We have

$$\Omega_{i,0}(t) = \omega_e(x_i, y_0, t) + O(h^4),$$

$$U_{i,j}(t) = u_e(x_i, y_j, t) + O(h^4), \qquad (4.10)$$

$$V_{ij}(t) = v_e(x_i, y_j, t) + O(h^4).$$

$$\psi_e(x_i, y_{-1}) = 6\psi_e(x_i, y_1) - 2\psi_e(x_i, y_2) + \frac{1}{3}\psi_e(x_i, y_3)$$

$$- \frac{h^5}{5} \partial_y^5 \psi_e(x_i, y_0) + O(h^6),$$

$$(4.11)$$

where $y_{-1} = -h$. Similarly, using the fact that

$$\hat{\psi}|_\Gamma = 0, \qquad (4.12)$$

we also have

$$\hat{\psi}(x_i, y_{-1}) = 6\hat{\psi}(x_i, y_1) - 2\hat{\psi}(x_i, y_2) + \frac{1}{3}\hat{\psi}(x_i, y_3)$$
$$+ 4h\partial_y\hat{\psi}(x_i, y_0) + O(h^2). \qquad (4.13)$$

Hence from (4.2), (4.11)–(4.12) we have

$$\bar{\psi}(x_i, y_{-1}) = 6\bar{\psi}(x_i, y_1) - 2\bar{\psi}(x_i, y_2)$$
$$+ \frac{1}{3}\bar{\psi}(x_i, y_3) + O(h^6). \qquad (4.14)$$

For the boundary vorticity we have

$$\bar{\omega}(x_i, y_0) = \partial_x^2 \bar{\psi}(x_i, y_0) = \frac{1}{12h^2}(11\bar{\psi}(x_i, y_{-1}) + 6\bar{\psi}(x_i, y_1)$$
$$+ 4\bar{\psi}(x_i, y_2) - \bar{\psi}(x_i, y_3)) + O(h^4).$$
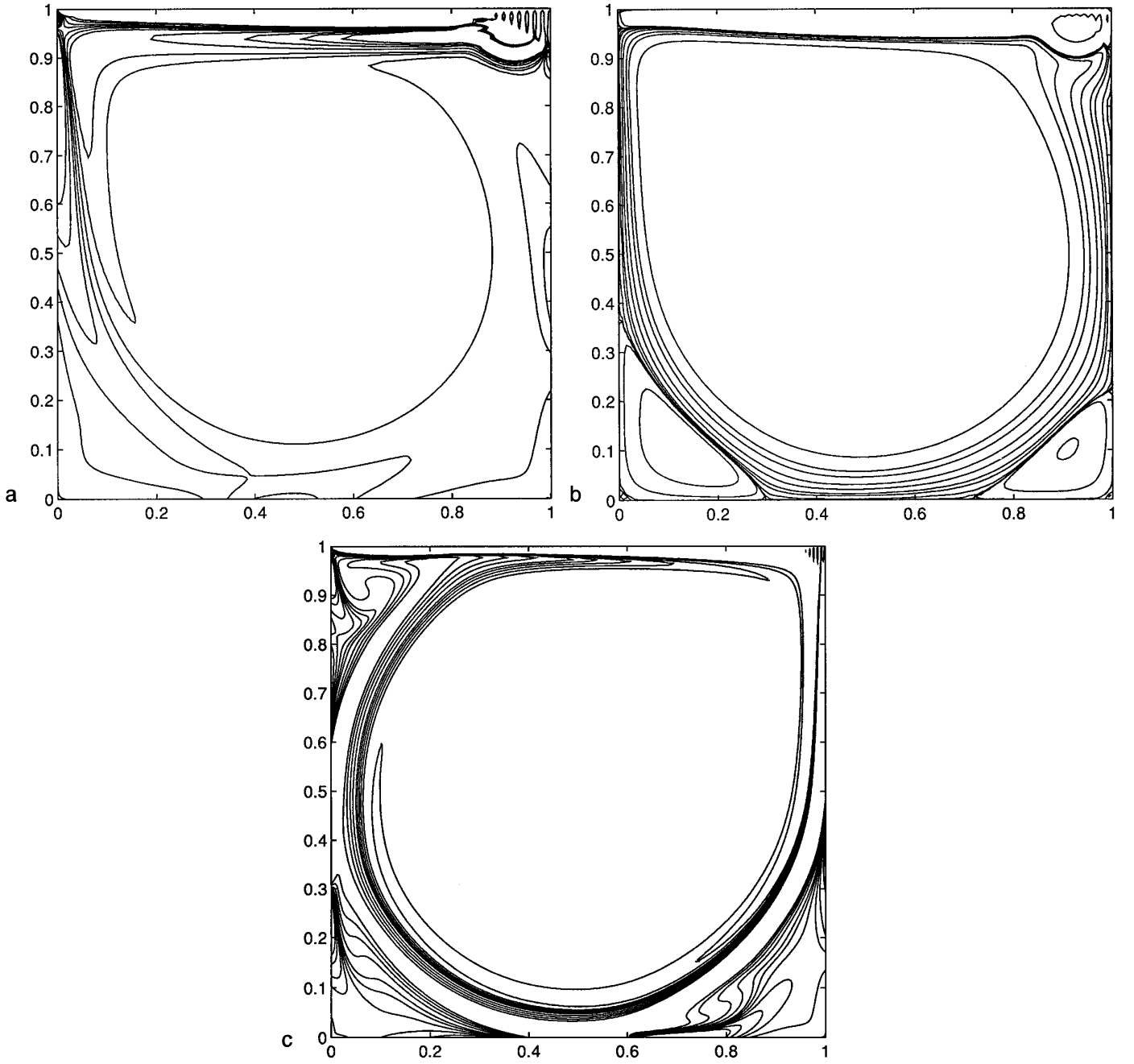
Using (4.14), this becomes

$$\bar{\omega}(x_i, y_0, t) = \frac{1}{18h^2}(108\Psi_{i,1} - 27\Psi_{i,2} + 4\Psi_{i,3})$$
$$+ O(h^4) = \Omega_{i,0} + O(h^4).$$

(This is an alternative way of deriving Briley's formula.) This implies

$$\Omega_{i,0} = \omega_e(x_i, y_0, t) + O(h^4). \qquad (4.15)$$

We also have

$$\bar{\Omega}_{i,j} = \left(\Delta_h + \frac{h^2}{6} D_x^2 D_y^2\right)\Psi_{i,j}$$
$$= \Delta\bar{\psi}(x_i, y_j) + \frac{h^2}{12}(\partial_x^4 + \partial_y^4)\bar{\psi}(x_i, y_j)$$
$$+ \frac{h^2}{6}\partial_x^2\partial_y^2\bar{\psi}(x_i, y_j) + O(h^4) \qquad (4.16)$$
$$= \Delta\psi_e(x_i, y_j) + \frac{h^2}{12}\Delta^2(x_i, y_j) + O(h^4)$$

FIG. 6. Contour plot of vorticity at Reynolds number 10^5 computed using EC4. Other parameters: $n = 512$, $t = 2$.

Proof. We will drop the time variable t in the proof. Using Taylor expansion and the fact that

$$\psi_e|_\Gamma = \frac{\partial\psi_e}{\partial y}\Big|_\Gamma = 0$$

we have

FIG. 7. Resolution of the boundary layer for EC4. Shown in the figure is the horizontal cut of vorticity at $y = 0.5$. Grid points are shown in "x." Other parameters: $n = 1024$, $t = 2$.

FIG. 8. (a) Contour plot of vorticity for the case when $u_b(x) = 1$ computed using the second-order scheme. Other parameters: $n = 128$, $t = 400$. (b) Contour plot of vorticity for the case when $u_b(x) = 1$ computed using EC4. Other parameters: $n = 128$, $t = 400$. (c) Contour plot of vorticity for the case when $u_b(x) = 1$ computed using the second-order method. Other parameters: $n = 256$, $t = 400$.

$$= \left(1 + \frac{h^2}{12}\Delta\right)\omega_e(x_i, y_j) + O(h^4)$$

$$= \left(1 + \frac{h^2}{12}\Delta_h\right)\omega_e(x_i, y_j) + O(h^4).$$

Therefore we get

$$\left(1 + \frac{h^2}{12}\Delta_h\right)(\Omega_{i,j} - \omega_e(x_i, y_j)) = O(h^4),$$

$$(\Omega - \omega_e)|_\Gamma = O(h^4).$$

Since the matrix $I + (h^2/12)\Delta_h$ is uniformly diagonal dominant, we have

$$\Omega_{i,j} = \omega_e(x_i, y_j) + O(h^4). \qquad (4.17)$$

This proves the first inequality of (4.10). The rest follows directly from (4.5) and (4.6), and the fact that

$$\Psi_{i,-1}(t) = \psi_e(x_i, y_{-1}, t) + h^4\hat{\psi}(x_i, y_{-1}, t) + O(h^6). \quad (4.18)$$

This completes the proof of the lemma.

Finally we compute the truncation error in the momentum equation. At $(x_i, y_j), 0 \le i \le M, 1 \le j \le N-1$, we have

$$\left(1 + \frac{h^2}{12}\Delta_h\right)\partial_t\Omega + \tilde{D}_x\left(1 + \frac{h^2}{6}D_y^2\right)(U\Omega)$$

$$+ \tilde{D}_y\left(1 + \frac{h^2}{6}D_x^2\right)(V\Omega)$$

$$- \frac{h^2}{12}\Delta_h(U\tilde{D}_x\Omega + V\tilde{D}_x\Omega) - \nu\left(\Delta_h + \frac{h^2}{6}D_x^2D_y^2\right)\Omega$$

$$= \left(1 + \frac{h^2}{12}\Delta\right)\partial_t\omega + \partial_x\left(1 + \frac{h^2}{6}\partial_x^2\right)\left(1 + \frac{h^2}{6}\partial_y^2\right)(u\omega)$$

$$+ \partial_y\left(1 + \frac{h^2}{6}\partial_y^2\right)\left(1 + \frac{h^2}{6}\partial_x^2\right)(v\omega)$$

$$- \frac{h^2}{12}\Delta(u\partial_x\omega + v\partial_y\omega) - \nu\left(\Delta + \frac{h^2}{12}(\partial_x^4 \qquad (4.19)\right.$$

$$\left. + \partial_y^4) + \frac{h^2}{6}\partial_x^2\partial_y^2\right)\omega + O(h^4)$$

$$= \left(1 + \frac{h^2}{12}\Delta\right)\partial_t\omega + \left(1 + \frac{h^2}{6}\Delta\right)\partial_x(u\omega)$$

$$+ \left(1 + \frac{h^2}{6}\Delta\right)\partial_y(v\omega)$$

$$- \frac{h^2}{12}\Delta(u\partial_x\omega + v\partial_y\omega) - \nu\left(1 + \frac{h^2}{12}\Delta\right)\Delta\omega + O(h^4)$$

$$= \left(1 + \frac{h^2}{12}\Delta\right)(\partial_t\omega + u\partial_x\omega + v\partial_y\omega - \nu\Delta\omega) + O(h^4)$$

$$= O(h^4).$$

Here U and V are defined by (4.6) and hence smooth up to the boundary. At the boundary they vanish up to $O(h^4)$.

4.2. Stability and Error Estimates

The initial condition for the numerical solution $\{\psi_{i,j}(t)\}$ is taken to be: $\psi_{i,j}(0) = \psi_e(x_i, y_j, 0)$. Define

$$\tilde{\psi}_{i,j} = \psi_{i,j} - \Psi_{i,j}, \quad \tilde{\omega}_{i,j} = \omega_{i,j} - \Omega_{i,j},$$
$$\tilde{u}_{i,j} = u_{i,j} - U_{i,j}, \quad \tilde{v}_{i,j} = v_{i,j} - V_{i,j}. \qquad (4.20)$$

We have from (4.19) that

$$\left(1 + \frac{h^2}{12}\Delta_h\right)\partial_t\tilde{\omega} - \nu\left(\Delta_h + \frac{h^2}{6}D_x^2D_y^2\right)\tilde{\omega}$$

$$= -\tilde{D}_x\left(1 + \frac{h^2}{6}D_y^2\right)(\tilde{u}\Omega + u\tilde{\omega})$$

$$- \tilde{D}_y\left(1 + \frac{h^2}{6}D_x^2\right)(\tilde{v}\Omega + v\tilde{\omega}) \qquad (4.21)$$

$$+ \frac{h^2}{12}\Delta_h(u\tilde{D}_x\tilde{\omega} + v\tilde{D}_y\tilde{\omega})$$

$$+ \frac{h^2}{12}\Delta_h(\tilde{u}\tilde{D}_x\Omega + \tilde{v}\tilde{D}_y\Omega) + O(h^4).$$

From (4.7) and (4.8), we have

$$\left(\Delta_h + \frac{h^2}{6}D_x^2D_y^2\right)\tilde{\psi} = \left(1 + \frac{h^2}{12}\Delta_h\right)\tilde{\omega}. \qquad (4.22)$$

From (4.5) and (4.6), we obtain

$$\tilde{u} = -\tilde{D}_y\left(1 - \frac{h^2}{6}D_y^2\right)\tilde{\psi}, \quad \tilde{v} = \tilde{D}_x\left(1 - \frac{h^2}{6}D_x^2\right)\tilde{\psi}. \quad (4.23)$$

From (4.3), (4.4), and (4.5), we have

$$\tilde{\psi}_{i,0} = \tilde{\psi}_{i,N} = 0, \qquad (4.24)$$

$$\tilde{\psi}_{i,-1} = 6\tilde{\psi}_{i,1} - 2\tilde{\psi}_{i,2} + \tfrac{1}{3}\tilde{\psi}_{i,3} \qquad (4.25)$$

and

$$\tilde{\omega}_{i,0} = \frac{1}{18h^2}(108\tilde{\psi}_{i,1} - 27\tilde{\psi}_{i,2} + 4\tilde{\psi}_{i,3}). \qquad (4.26)$$

Notice that the error functions satisfy the boundary conditions in the numerical exactly.

The basic strategy in estimating the error is to multiply (4.21) by $-(1 + (h^2/12)\Delta_h)\tilde{\psi}_{ij}$, sum by parts, and estimate the results with special care to the boundary terms. This is done in several steps which we put together as lemmas. We will use the discrete L^2-inner product

$$\langle u, v \rangle = \sum_{\substack{0 \le i \le N-1 \\ 1 \le j \le N-1}} u_{i,j}v_{i,j}h^2 \qquad (4.27)$$

and the discrete L^2-norm

$$\|u\| = \langle u, u \rangle^{1/2}. \tag{4.28}$$

LEMMA 4.2.   *The following identities hold:*

$$-\left\langle \left(1 + \frac{h^2}{12}\Delta_h\right)\tilde{\psi}, \left(1 + \frac{h^2}{12}\Delta_h\right)\partial_t\tilde{\omega}\right\rangle$$

$$= \frac{1}{2}\frac{d}{dt}\left(\|\nabla_h\tilde{\psi}\|^2 - \frac{h^2}{12}\|\Delta_h\tilde{\psi}\|^2 - \frac{h^2}{6}\|D_xD_y\tilde{\psi}\|^2\right. \tag{4.29}$$

$$\left. + \frac{h^4}{72}(\|D_xD_y^2\tilde{\psi}\|^2 + \|D_yD_x^2\tilde{\psi}\|^2)\right)$$

and

$$\left\langle \left(1 + \frac{h^2}{12}\Delta_h\right)\tilde{\psi}, \left(\Delta_h + \frac{h^2}{6}D_x^2D_y^2\right)\tilde{\omega}\right\rangle$$

$$= \left\|\left(1 + \frac{h^2}{12}\Delta_h\right)\tilde{\omega}\right\|^2 + \sum_i\left(1 + \frac{h^2}{6}D_x^2 + \frac{h^4}{72}D_x^4\right)\tilde{\psi}_{i,1}\tilde{\omega}_{i,0}$$

$$+ \sum_i\left(1 + \frac{h^2}{6}D_x^2 + \frac{h^4}{72}D_x^4\right)\tilde{\psi}_{i,N-1}\tilde{\omega}_{i,N}. \tag{4.30}$$

Proof.   Using (4.22), (4.24), summing by parts, we have

$$\left\langle \left(1 + \frac{h^2}{12}\Delta_h\right)\tilde{\psi}, \left(1 + \frac{h^2}{12}\Delta_h\right)\partial_t\tilde{\omega}\right\rangle$$

$$= \left\langle \left(1 + \frac{h^2}{12}\Delta_h\right)\tilde{\psi}, \left(\Delta_h + \frac{h^2}{6}D_x^2D_y^2\right)\partial_t\tilde{\psi}\right\rangle$$

$$\tag{4.31}$$

$$= \langle\tilde{\psi}, \Delta_h\partial_t\tilde{\psi}\rangle + \frac{h^2}{12}\langle\Delta_h\tilde{\psi}, \Delta_h\partial_t\tilde{\psi}\rangle + \frac{h^2}{6}\langle\tilde{\psi}, D_x^2D_y^2\partial_t\tilde{\psi}\rangle$$

$$+ \frac{h^2}{72}\langle\Delta_h\tilde{\psi}, D_x^2D_y^2\partial_t\tilde{\psi}\rangle.$$

Summing by parts and using (4.24) we have

$$\langle\tilde{\psi}, \Delta_h\partial_t\tilde{\psi}\rangle = -\frac{1}{2}\frac{d}{dt}\|\nabla_h\tilde{\psi}\|^2,$$

$$\langle\tilde{\psi}, D_x^2D_y^2\partial_t\tilde{\psi}\rangle = \frac{1}{2}\frac{d}{dt}\|D_xD_y\tilde{\psi}\|^2,$$

$$\langle\Delta_h\tilde{\psi}, D_x^2D_y^2\partial_t\tilde{\psi}\rangle = \langle D_x^2\tilde{\psi}, D_x^2D_y^2\partial_t\tilde{\psi}\rangle + \langle D_y^2\tilde{\psi}, D_x^2D_y^2\partial_t\tilde{\psi}\rangle$$

$$= \frac{1}{2}\frac{d}{dt}(\|D_yD_x^2\tilde{\psi}\|^2 + \|D_xD_y^2\tilde{\psi}\|^2).$$

In the last equality we used the fact that $D_x^2\psi|_{j=0,N} = 0$ since $\tilde{\psi}|_{j=0,N} = 0$. This proves (4.29). In order to prove (4.30), we need to switch the difference operators acting on $\tilde{\psi}$ and $\tilde{\omega}$ on the left-hand side of (4.30). Boundary term

occurs when we sum by parts the D_y operator. Using (4.24)–(4.26), we have

$$\left\langle \left(1 + \frac{h^2}{12}\Delta_h\right)\tilde{\psi}, \left(\Delta_h + \frac{h^2}{6}D_x^2D_y^2\right)\tilde{\omega}\right\rangle$$

$$= \left\langle \left(1 + \frac{h^2}{12}D_x^2 + \frac{h^2}{12}D_y^2\right)\tilde{\psi}, \left(D_x^2 + \left(1 + \frac{h^2}{6}D_x^2\right)D_y^2\right)\tilde{\omega}\right\rangle$$

$$= \left\langle \left(1 + \frac{h^2}{12}D_x^2\right)\tilde{\psi}, D_x^2\tilde{\omega}\right\rangle + \frac{h^2}{12}\left\langle D_y^2\tilde{\psi}, \right.$$

$$\left.\left(1 + \frac{h^2}{6}D_x^2\right)D_y^2\tilde{\omega}\right\rangle + \frac{h^2}{12}\left\langle D_y^2\tilde{\psi}, D_x^2\tilde{\omega}\right\rangle$$

$$+ \left\langle \left(1 + \frac{h^2}{12}D_x^2\right)\tilde{\psi}, \left(1 + \frac{h^2}{6}D_x^2\right)D_y^2\tilde{\omega}\right\rangle.$$

We always have

$$\left\langle \left(1 + \frac{h^2}{12}D_x^2\right)\tilde{\psi}, D_x^2\tilde{\omega}\right\rangle = \left\langle D_x^2\tilde{\psi}, \left(1 + \frac{h^2}{12}D_x^2\right)\tilde{\omega}\right\rangle.$$

Since

$$\left\langle \left(1 + \frac{h^2}{12}D_x^2\right)\tilde{\psi}, \left(1 + \frac{h^2}{6}D_x^2\right)D_y^2\tilde{\omega}\right\rangle$$

$$= \left\langle \left(1 + \frac{h^2}{6}D_x^2\right)\tilde{\psi}, D_y^2\tilde{\omega}\right\rangle + \frac{h^2}{12}\langle D_x^2\tilde{\psi}, D_y^2\tilde{\omega}\rangle$$

$$+ \frac{h^4}{72}\langle D_x^2\tilde{\psi}, D_x^2D_y^2\tilde{\omega}\rangle$$

$$= \frac{h^2}{12}\langle D_x^2\tilde{\psi}, D_y^2\tilde{\omega}\rangle + \left\langle \left(1 + \frac{h^2}{6}D_x^2 + \frac{h^4}{72}D_x^4\right)\tilde{\psi}, D_y^2\tilde{\omega}\right\rangle$$

and

$$\left\langle \left(1 + \frac{h^2}{6}D_x^2 + \frac{h^4}{72}D_x^4\right)\tilde{\psi}, D_y^2\tilde{\omega}\right\rangle$$

$$= \left\langle D_y^2\tilde{\psi}, \left(1 + \frac{h^2}{6}D_x^2 + \frac{h^4}{72}D_x^4\right)\tilde{\omega}\right\rangle$$

$$+ \sum_i\left(1 + \frac{h^2}{6}D_x^2 + \frac{h^4}{72}D_x^4\right)\tilde{\psi}_{i,1}\tilde{\omega}_{i,0}$$

$$+ \sum_i\left(1 + \frac{h^2}{6}D_x^2 + \frac{h^4}{72}D_x^4\right)\tilde{\psi}_{i,N-1}\tilde{\omega}_{i,N},$$

we get

$$\left\langle\left(1+\frac{h^2}{12}D_x^2\right)\tilde\psi,\left(1+\frac{h^2}{6}D_x^2\right)D_y^2\tilde\omega\right\rangle$$

$$=\left\langle\left(1+\frac{h^2}{6}D_x^2\right)D_y^2\tilde\psi,\left(1+\frac{h^2}{12}D_x^2\right)\tilde\omega\right\rangle$$

$$+\sum_i\left(1+\frac{h^2}{6}D_x^2+\frac{h^4}{72}D_x^4\right)\tilde\psi_{i,1}\tilde\omega_{i,0}$$

$$+\sum_i\left(1+\frac{h^2}{6}D_x^2+\frac{h^4}{72}D_x^4\right)\tilde\psi_{i,N-1}\tilde\omega_{i,N}.$$

Other terms can be dealt with similarly. Now using (4.22) and (4.26) we prove (4.30).

LEMMA 4.3. *We have*

$$\|D_y^2\tilde\psi\|^2\le\left\|\left(1+\frac{h^2}{12}\Delta_h\right)\tilde\omega\right\|^2,\qquad(4.32)$$

$$\|\tilde\omega\|^2\le\frac{6}{5}\left\|\left(1+\frac{h^2}{12}\Delta_h\right)\tilde\omega\right\|^2,\qquad(4.33)$$

$$\left\|\left(1+\frac{h^2}{6}D_x^2+\frac{h^4}{72}D_x^4\right)D_y^2\tilde\psi\right\|^2\le\|D_y^2\tilde\psi\|^2.\qquad(4.34)$$

Proof. Since $\{\tilde\psi_{i,j}\}$ is periodic in i and zero for $j=0$, N, we can Fourier transform $\{\tilde\psi_{i,j}\}$ in the i-direction and sine transform it in the j-direction, i.e.,

$$\tilde\psi_{i,j}=\sum_{k,l}\hat{\tilde\psi}_{k,l}\,e^{2\pi ikx_i}\sin(l\pi y_j).\qquad(4.35)$$

Parserval equality gives

$$\sum_{i,j}(\tilde\psi_{i,j})^2=\sum_{k,l}|\hat{\tilde\psi}_{k,l}|^2.\qquad(4.36)$$

We neglect the constants in front of the summation since they do not affect the result. Let

$$f_k=-\frac{4}{h^2}\sin^2\left(\frac{2\pi kh}{2}\right),\quad g_l=-\frac{4}{h^2}\sin^2\left(\frac{l\pi h}{2}\right),\quad(4.37)$$

we have

$$D_x^2\tilde\psi_{i,j}=\sum_{k,l}f_k\,\hat{\tilde\psi}_{k,l},\quad D_y^2\tilde\psi_{i,j}=\sum_{k,l}g_l\,\hat{\tilde\psi}_{k,l}.\qquad(4.38)$$

Since $1-(h^2/6)g_l\ge0$, we have

$$\sum_{i,j}\left|\left(1+\frac{h^2}{12}\Delta_h\right)\tilde\omega_{i,j}\right|^2=\sum_{i,j}\left|\left(\Delta_h+\frac{h^2}{6}D_x^2D_y^2\right)\tilde\psi_{i,j}\right|^2$$

$$=\sum_{k,l}\left|g_l+f_k\left(1-\frac{h^2}{6}g_l\right)\right|^2|\hat{\tilde\psi}_{k,l}|^2$$

$$\ge\sum_{k,l}g_l^2|\hat{\tilde\psi}_{k,l}|^2=\sum_{i,j}\|D_y^2\tilde\psi_{i,j}\|^2.$$

Similarly, since $x=\sin^2(k\Delta x/2)\in[0,1]$, we have

$$\sum_{i,j}\left|\left(1+\frac{h^2}{6}D_x^2+\frac{h^4}{72}D_x^4\right)D_y^2\tilde\psi_{i,j}\right|^2$$

$$=\sum_{k,l}g_l^2\left(1+\frac{h^2}{6}f_k+\frac{h^4}{72}f_k^2\right)^2|\hat{\tilde\psi}_{k,l}|^2$$

$$=\max_{0\le x\le1}\left(1-\frac{2x}{3}+\frac{2x^2}{9}\right)^2\sum_{k,l}g_l^2|\hat{\tilde\psi}_{k,l}|^2$$

$$\le\sum_{i,j}|D_y^2\tilde\psi_{i,j}|^2.$$

The proof of (4.33) is similar. This completes the proof of the lemma.

LEMMA 4.4. (Estimate of the boundary terms).

$$\sum_i\left(1+\frac{h^2}{6}D_x^2+\frac{h^4}{72}D_x^4\right)\tilde\psi_{i,1}\tilde\omega_{i,0}$$

$$+\sum_i\left(1+\frac{h^2}{6}D_x^2+\frac{h^4}{72}D_x^4\right)\tilde\psi_{i,N-1}\tilde\omega_{i,N}\quad(4.39)$$

$$\ge-\frac{1}{2}\|D_y^2\tilde\psi\|^2.$$

Proof. We have

$$\frac{1}{18h^2}\sum_i\left(1+\frac{h^2}{6}D_x^2+\frac{h^4}{72}D_x^4\right)\tilde\psi_{i,1}$$

$$\times(108\tilde\psi_{i,1}-27\tilde\psi_{i,2}+4\tilde\psi_{i,3})$$

$$=\frac{1}{18h^2}\sum_i\left(1+\frac{h^2}{6}D_x^2+\frac{h^4}{72}D_x^4\right)\tilde\psi_{i,1}$$

$$\times(66\tilde\psi_{i,1}-19h^2(D_y^2\tilde\psi)_{i,1}+4h^2(D_y^2\tilde\psi)_{i,2})$$

$$=\frac{11}{3h^2}\sum_i\left(|\tilde\psi_{i,1}|^2+\frac{h^2}{6}\tilde\psi_{i,1}D_x^2\tilde\psi_{i,1}+\frac{h^4}{72}|D_x^2\tilde\psi_{i,1}|^2\right)$$

$$-\frac{19}{18}\sum_i\tilde\psi_{i,1}\left(1+\frac{h^2}{6}D_x^2+\frac{h^4}{72}D_x^4\right)(D_y^2\tilde\psi)_{i,1}$$

$$+\frac{2}{9}\sum_i\tilde\psi_{i,1}\left(1+\frac{h^2}{6}D_x^2+\frac{h^4}{72}D_x^4\right)(D_y^2\tilde\psi)_{i,2}.$$

We also have

$$|\tilde{\psi}_{i,1}|^2 + \frac{h^2}{6}\tilde{\psi}_{i,1}D_x^2\tilde{\psi}_{i,1} + \frac{h^4}{72}|D_x^2\tilde{\psi}_{i,1}|^2$$

$$\geq |\tilde{\psi}_{i,1}|^2 - \frac{1}{2}|\tilde{\psi}_{i,1}|^2 - \frac{h^4}{72}|D_x^2\tilde{\psi}_{i,1}|^2$$

$$+ \frac{h^4}{72}|D_x^2\tilde{\psi}_{i,1}|^2 \geq \frac{1}{2}|\tilde{\psi}_{i,1}|^2,$$

$$-\frac{19}{18}\tilde{\psi}_{i,1}\left(1 + \frac{h^2}{6}D_x^2 + \frac{h^4}{72}D_x^4\right)(D_y^2\tilde{\psi})_{i,1}$$

$$\geq -\frac{1}{2h^2}\frac{19^2}{18^2}|\tilde{\psi}_{i,1}|^2 - \frac{1}{2}\left|\left(1 + \frac{h^2}{6}D_x^2\right.\right.$$

$$\left.\left.+ \frac{h^4}{72}D_x^4\right)(D_y^2\tilde{\psi})_{i,1}\right|^2 h^2,$$

and

$$\frac{2}{9}\sum_i \tilde{\psi}_{i,1}\left(1 + \frac{h^2}{6}D_x^2 + \frac{h^4}{72}D_x^4\right)(D_y^2\tilde{\psi})_{i,2}$$

$$\geq -\frac{1}{2h^2}\frac{2^2}{9^2}|\tilde{\psi}_{i,1}|^2 - \frac{1}{2}\left|\left(1 + \frac{h^2}{6}D_x^2 + \frac{h^4}{72}D_x^4\right)(D_y^2\tilde{\psi})_{i,2}\right|^2 h^2.$$

Since $\frac{11}{6} - \frac{1}{2}(19^2/18^2 + \frac{4}{81}) \geq 0$, we have

$$\frac{1}{18h^2}\sum_i\left(1 + \frac{h^2}{6}D_x^2 + \frac{h^4}{72}D_x^4\right)\tilde{\psi}_{i,1}(108\tilde{\psi}_{i,1} - 27\tilde{\psi}_{i,2} + 4\tilde{\psi}_{i,3})$$

$$\geq -\frac{1}{2}\sum_i\sum_{j=1,2}\left|\left(1 + \frac{h^2}{6}D_x^2 + \frac{h^4}{72}D_x^4\right)D_y^2\tilde{\psi}_{i,j}\right|^2 h^2.$$

The treatment of the second term on the left-hand side of (4.39) is exactly the same. Now using (4.34) we get the left-hand side of (4.39)

$$\geq -\frac{1}{2}\sum_i\sum_{j=1,2,N-2,N-1}\left|\left(1 + \frac{h^2}{6}D_x^2 + \frac{h^4}{72}D_x^4\right)D_y^2\tilde{\psi}_{i,j}\right|^2 h^2$$

$$\geq -\frac{1}{2}\sum_{i,j}\left|\left(1 + \frac{h^2}{6}D_x^2 + \frac{h^4}{72}D_x^4\right)D_x^2\tilde{\psi}_{i,j}\right|^2 h^2 \geq -\frac{1}{2}\|D_y^2\tilde{\psi}_{i,j}\|^2.$$

This completes the proof of the lemma.

LEMMA 4.5. (Estimate of the linearized convection term). *Assume that the numerical solution satisfies a uniform bound*

$$\max_{0 \leq t \leq T, i, j}|\mathbf{u}_{i,j}(t)| \leq C_0, \tag{4.40}$$

then we have

$$\left\langle\left(1 + \frac{h^2}{12}\Delta_h\right)\tilde{\psi}, \tilde{D}_x\left(1 + \frac{h^2}{6}D_y^2\right)(\tilde{u}\Omega + u\tilde{\omega})\right\rangle$$

$$\leq C_\nu\|\tilde{\mathbf{u}}\|^2 + \frac{\nu}{12}\|\tilde{\omega}\|^2, \tag{4.41}$$

$$\left\langle\left(1 + \frac{h^2}{12}\Delta_h\right)\tilde{\psi}, \tilde{D}_y\left(1 + \frac{h^2}{6}D_x^2\right)(\tilde{v}\Omega + v\tilde{\omega})\right\rangle$$

$$\leq C_\nu\|\tilde{\mathbf{u}}\|^2 + \frac{\nu}{12}\|\tilde{\omega}\|^2, \tag{4.42}$$

$$-\frac{h^2}{12}\left\langle\left(1 + \frac{h^2}{12}\Delta_h\right)\tilde{\psi}, \Delta_h(u\tilde{D}_x\tilde{\omega} + v\tilde{D}_x\tilde{\omega})\right\rangle$$

$$\leq C_\nu\|\tilde{\mathbf{u}}\|^2 + \frac{\nu}{12}\|\tilde{\omega}\|^2, \tag{4.43}$$

and

$$-\frac{h^2}{12}\left\langle\left(1 + \frac{h^2}{12}\Delta_h\right)\tilde{\psi}, \Delta_h(\tilde{u}\tilde{D}_x\Omega + \tilde{v}\tilde{D}_x\Omega)\right\rangle$$

$$\leq \mathbf{C}_\nu\|\tilde{\mathbf{u}}\|^2 + \frac{\nu}{12}\|\tilde{\omega}\|^2 \tag{4.44}$$

where $\tilde{\mathbf{u}} = (\tilde{u}, \tilde{v})$ and C_ν depends on C_0 and ν.

Proof. We first prove (4.41). Summing by parts, we have

$$\left\langle\left(1 + \frac{h^2}{12}\Delta_h\right)\tilde{\psi}, \tilde{D}_x\left(1 + \frac{h^2}{6}D_y^2\right)(\tilde{u}\Omega + u\tilde{\omega})\right\rangle$$

$$= \frac{h^2}{12}\left\langle\Delta_h\tilde{\psi}, \tilde{D}_x\left(1 + \frac{h^2}{6}D_y^2\right)(\tilde{u}\Omega + u\tilde{\omega})\right\rangle$$

$$- \left\langle\tilde{D}_x\tilde{\psi}, \left(1 + \frac{h^2}{6}D_y^2\right)(\tilde{u}\Omega + u\tilde{\omega})\right\rangle.$$

Notice that

$$\frac{h^2}{12}\left\langle\Delta_h\tilde{\psi}, \tilde{D}_x\left(1 + \frac{h^2}{6}D_y^2\right)(\tilde{u}\Omega + u\tilde{\omega})\right\rangle$$

$$\leq \frac{1}{12}\|h\Delta_h\tilde{\psi}\|\left\|h\tilde{D}_x\left(1 + \frac{h^2}{6}D_y^2\right)(\tilde{u}\Omega + u\tilde{\omega})\right\|$$

$$\leq C\|\nabla_h\tilde{\psi}\|\left\|\left(1 + \frac{h^2}{6}D_y^2\right)(\tilde{u}\Omega + u\tilde{\omega})\right\|$$

$$\leq C\|\tilde{D}_x\tilde{\psi}\|(\|\tilde{u}\| + \|\tilde{\omega}\|).$$

In the last inequality we have used (4.40). Similarly,

$$\left\langle \tilde{D}_x\tilde{\psi}, \left(1 + \frac{h^2}{6}D_y^2\right)(\tilde{u}\Omega + u\tilde{\omega})\right\rangle \le C\|\tilde{D}_x\tilde{\psi}\|(\|\tilde{u}\| + \|\tilde{\omega}\|).$$

Hence

$$\left\langle \left(1 + \frac{h^2}{12}\Delta_h\right)\tilde{\psi}, \tilde{D}_x\left(1 + \frac{h^2}{6}D_y^2\right)(\tilde{u}\Omega + u\tilde{\omega})\right\rangle$$

$$\le C(\|\tilde{\mathbf{u}}\|^2 + \|\tilde{\mathbf{u}}\|\,\|\tilde{\omega}\|) \le C_\nu\|\tilde{\mathbf{u}}\|^2 + \frac{\nu}{12}\|\tilde{\omega}\|^2.$$

This gives (4.41). Now we prove (4.43). Clearly

$$-\frac{h^4}{12^2}\left\langle \Delta_h\tilde{\psi}, \Delta_h(u\tilde{D}_x\tilde{\omega} + v\tilde{D}_x\tilde{\omega})\right\rangle \le C_\nu\|\tilde{\mathbf{u}}\|^2 + \frac{\nu}{12}\|\tilde{\omega}\|^2.$$

Hence,

$$-\frac{h^2}{12}\left\langle \left(1 + \frac{h^2}{12}\Delta_h\right)\tilde{\psi}, \Delta_h(u\tilde{D}_x\tilde{\omega} + v\tilde{D}_x\tilde{\omega})\right\rangle$$

$$\le -\frac{h^2}{12}\langle \tilde{\psi}, \Delta_h(u\tilde{D}_x\tilde{\omega} + v\tilde{D}_x\tilde{\omega})\rangle + C_\nu\|\tilde{\mathbf{u}}\|^2 + \frac{\nu}{12}\|\tilde{\omega}\|^2,$$

Since $\tilde{\psi} = 0$ on the boundary, the first term on the right hand side can be summed by parts to become

$$-\frac{h^2}{12}\langle \tilde{\psi}, \Delta_h(u\tilde{D}_x\tilde{\omega} + v\tilde{D}_x\tilde{\omega})\rangle$$

$$= \frac{h^2}{12}\langle D_x^+\tilde{\psi}, D_x^-(u\tilde{D}_x\tilde{\omega} + v\tilde{D}_x\tilde{\omega})\rangle$$

$$+ \frac{h^2}{12}\langle D_y^+\tilde{\psi}, D_y^-(u\tilde{D}_x\tilde{\omega} + v\tilde{D}_x\tilde{\omega})\rangle$$

$$\le C_\nu\|\tilde{\mathbf{u}}\|^2 + \frac{\nu}{12}\|\tilde{\omega}\|^2.$$

Here $D_x^\pm$ are forward and backward difference operators, respectively. This gives (4.43). The estimate of (4.44) is similar. The lemma is proved.

Now we prove our main theorem.

Proof. We first prove Theorem 1, assuming that (4.40) holds. Multiplying (4.21) by $-(1 + (h^2/12)\Delta_h)\tilde{\psi}$ and using Lemma 4.5, we have

$$-\left\langle \left(1 + \frac{h^2}{12}\Delta_h\right)\tilde{\psi}, \left(1 + \frac{h^2}{12}\Delta_h\right)\partial_t\tilde{\omega}\right\rangle$$

$$+ \nu\left\langle \left(1 + \frac{h^2}{12}\Delta_h\right)\tilde{\psi}, \left(\Delta_h + \frac{h^2}{6}D_x^2D_y^2\right)\tilde{\omega}\right\rangle$$

$$= \left\langle \left(1 + \frac{h^2}{12}\Delta_h\right)\tilde{\psi}, \tilde{D}_x\left(1 + \frac{h^2}{6}D_y^2\right)(\tilde{u}\Omega + u\tilde{\omega})\right\rangle$$

$$+ \left\langle \left(1 + \frac{h^2}{12}\Delta_h\right)\tilde{\psi}, \tilde{D}_y\left(1 + \frac{h^2}{6}D_x^2\right)(\tilde{v}\Omega + v\tilde{\omega})\right\rangle$$

$$- \frac{h^2}{12}\left\langle \left(1 + \frac{h^2}{12}\Delta_h\right)\tilde{\psi}, \Delta_h(u\tilde{D}_x\tilde{\omega} + v\tilde{D}_x\tilde{\omega})\right\rangle$$

$$- \frac{h^2}{12}\left\langle \left(1 + \frac{h^2}{12}\Delta_h\right)\tilde{\psi}, \Delta_h(\tilde{u}\tilde{D}_x\Omega + \tilde{v}\tilde{D}_x\Omega)\right\rangle$$

$$+ \sum_{i,j} O(h^4)\left|\left(1 + \frac{h^2}{12}\Delta_h\right)\tilde{\psi}_{ij}\right|h^2$$

$$\le C_\nu\|\tilde{\mathbf{u}}\|^2 + \frac{4\nu}{12}\|\tilde{\omega}\|^2 + O(h^8) + C\|\tilde{\psi}\|^2$$

$$\le O(h^8) + C\|\nabla_h\tilde{\psi}\|^2 + \frac{4\nu}{12}\|\tilde{\omega}\|^2.$$

Lemmas 4.2–4.4 imply

$$\left\langle \left(1 + \frac{h^2}{12}\Delta_h\right)\tilde{\psi}, \left(\Delta_h + \frac{h^2}{6}D_x^2D_y^2\right)\tilde{\omega}\right\rangle$$

$$\ge \left\|\left(1 + \frac{h^2}{12}\Delta_h\right)\tilde{\omega}\right\|^2 - \frac{1}{2}\|D_y^2\tilde{\psi}\|^2$$

$$\ge \frac{1}{2}\left\|\left(1 + \frac{h^2}{12}\Delta_h\right)\tilde{\omega}\right\|^2 \ge \frac{5}{12}\|\tilde{\omega}\|^2.$$

Together with Lemma 4.2, we have

$$\frac{1}{2}\frac{d}{dt}\left(\|\nabla_h\tilde{\psi}\|^2 - \frac{h^2}{12}\|\Delta_h\tilde{\psi}\|^2 - \frac{h^2}{6}\|D_xD_y\tilde{\psi}\|^2\right.$$

$$\left. + \frac{h^4}{72}(\|D_xD_y^2\tilde{\psi}\|^2 + \|D_yD_x^2\tilde{\psi}\|^2)\right)$$

$$\le O(h^8) + C\|\nabla_h\tilde{\psi}\|^2 + \frac{4\nu}{12}\|\tilde{\omega}\|^2 - \frac{5\nu}{12}\|\tilde{\omega}\|^2$$

$$\le O(h^8) + C\|\nabla_h\tilde{\psi}\|^2.$$

Integrating in time, we get

$$\|\nabla_h\tilde{\psi}\|^2 - \frac{h^2}{12}\|\Delta_h\tilde{\psi}\|^2 - \frac{h^2}{6}\|D_xD_y\tilde{\psi}\|^2$$

$$+ \frac{h^4}{72}(\|D_xD_y^2\tilde{\psi}\|^2 + \|D_yD_x^2\tilde{\psi}\|^2)$$

$$\leq O(h^8) + C \int_0^t \|\nabla_h \tilde{\psi}\|^2 \, dt.$$

Since

$$\|\nabla_h \tilde{\psi}\|^2 \leq 3\left(\|\nabla_h \tilde{\psi}\|^2 - \frac{h^2}{12} \|\Delta_h \tilde{\psi}\|^2 - \frac{h^2}{6} \|D_x D_y \tilde{\psi}\|^2 \right)$$

we get

$$\|\nabla_h \tilde{\psi}\|^2 \leq O(h^8) + C \int_0^t \|\nabla_h \tilde{\psi}\|^2 \, dt.$$

By the Gronwall inequality, we have

$$\|\nabla_h \tilde{\psi}\|^2 \leq O(h^8).$$

Thus, we have proved

$$\sup_{0 \leq t \leq T} \|\mathbf{u}(\cdot, t) - \mathbf{u}_h(\cdot, t)\|_{L^2} \leq Ch^4. \tag{4.45}$$

Using the inverse inequality, we have

$$\sup_{0 \leq t \leq T, i, j} |\mathbf{u}(x_i, y_j, t) - \mathbf{u}_{i,j}(t)| \leq Ch^3. \tag{4.46}$$

Now we can resort to a standard trick which asserts that (4.40) will never be violated if h is small enough. The theorem is proved.

5. CONCLUDING REMARKS

We presented a new essentially compact fourth-order scheme, together with ample numerical evidence of its superiority over the second-order scheme. We also presented a complete theory. The cost of this new fourth-order scheme is a little more than two times the cost of the second-order scheme. Since the complexity of the scheme is essentially the same as that of the second-order scheme, it can be used in all cases when the second-order scheme can be used, including cases when the geometry is reasonably complicated. Of course in such cases, we may not be able to use FFT. But we can still use other fast Poisson solvers developed for the *second-order* scheme, or more general fast solvers such as the multigrid method. In any case, the usually most complicated part of the code, the elliptic solver, is the same as in the second-order

method. Even for cases when the geometry itself cannot be specified to fourth-order accuracy, this fourth-order method may still have some advantage because of its small phase error. We also find it very encouraging that EC4 performed much better than the second-order method for the driven cavity flow when $u_b(x) = 1$, where there is a sharp singularity at the corners.

Perhaps the most exciting development brought about by EC4 is the possibility of exploring wall-bound flows at higher Reynolds number. Our preliminary study of the driven cavity flow at Reynolds number 10^6 has already shown some remarkable small scale structures. These are now being looked at in more detail.

REFERENCES

1. W. R. Briley, *J. Fluid Mech.* **47,** 713 (1971).
2. M. H. Carpenter, D. Gottlieb, and S. Abarbanel, *J. Comput. Phys.* **111,** 220 (1994).
3. S. C. R. Dennis and J. D. Hudson, *J. Comput. Phys.* **85,** 390 (1989).
4. W. E and J.-G. Liu, *J. Comput. Phys.* **124**(2), 301 (1996).
5. W. E and J.-G. Liu, preprint, 1995.
6. G. E. Forsythe and W. R. Wasow, *Finite-Difference Methods for Partial Differential Equations* (Wiley, New York, 1960).
7. U. Ghia, K. N. Ghia, and C. T. Shin, *J. Comput. Phys.* **48,** 387 (1982).
8. M. M. Gupta, *J. Comput. Phys.* **93,** 343 (1991).
9. W. D. Henshaw, H.-O. Kreiss, and L. G. M. Reyna, preprint, 1994.
10. T. Y. Hou and B. Wetton, *SIAM J. Numer. Anal.* 615 (1992).
11. B. C. Johansson, *J. Comput. Phys.* **105,** 233 (1993).
12. H.-O. Kreiss and J. Oliger, *Tellus* **24**(3), 199 (1972).
13. M. Li, T. Tang, and B. Fornberg, *Int. J. Numer. Methods Fluids* **20,** 1137 (1195).
14. K. Z. Meth, Ph.D. thesis, NYU, 1988 (unpublished).
15. K. Z. Meth, *SIAM J. Numer. Anal.* **31,** 1336 (1994).
16. M. J. Naughton, thesis, California Institute of Technology, 1986 (unpublished).
17. S. A. Orszag and M. Israeli, *Annu. Rev. Fluid Mech.* **6,** 281 (1974).
18. T. Phuoc Loc, *J. Fluid Mech.* **100,** 111 (1980).
19. M. B. Reider, Ph.D. thesis, UCLA, 1992 (unpublished).
20. R. Schreiber and H. B. Keller, *J. Comput. Phys.* **49,** 310 (1983).
21. G. Strang, *Numer. Math.* **6,** 37 (1964).
22. L. Wu and H.-O. Kreiss, preprint, 1991.